Journal of Materials Chemistry A

Accepted Manuscript

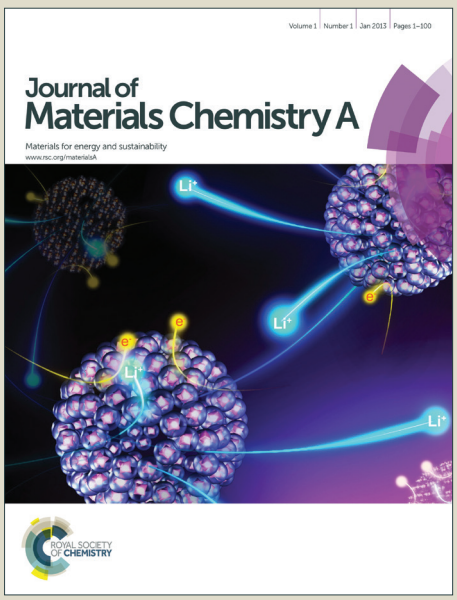

ROYAL SOCIETY OF CHEMISTRY

www.rsc.org/materialsA

Journal Name

RSCPublishing

ARTICLE

Prussian Blue Analogue: a New Class of Anode Material for Lithium Ion Batteries

Cite this: DOI: 10.1039/x0xx00000x

Ping Nie, Laifa Shen, Haifeng Luo, Bing Ding, Guiyin Xu, Jie Wang, and Xiaogang Zhang*

Received 00th January 2012,
Accepted 00th January 2012

DOI: 10.1039/x0xx00000x

www.rsc.org/

Metal-organic frameworks (MOFs) have attracted extensive interests in the context of energy storage duo to their high surface areas, controllable structures and excellent electrochemical properties. In particular, Prussian blue analogues (PBAs) have recently gained attention as a new class of cathode materials for rechargeable batteries. However, the anode properties of the host framework have been very limited. Herein, we demonstrate that nanoparticles of cobalt hexacyanocobaltate and manganese hexacyanocobaltate, typical Prussian blue analogues with the chemical formula $M_3^{II}[Co^{III}(CN)_6]_2 \cdot nH_2O$(M=Co, Mn), can be operated as novel battery anodes in an organic liquid-carbonate electrolyte. The $Co_3[Co(CN)_6]_2$ material exhibits a clear electrochemical activity in the voltage range of 0.01-3 V *vs*. Li/Li$^+$ with a reversible capacity of 299.1 mAh g^{-1}. Furthermore, superior rate capability (as the current density increases from 20 to 2000 mA g^{-1}, the capacity retains about 34%) could be achieved, attributing to the small particle sizes and rapid transport of Li$^+$ ions through large channels in the open-framework. We believe that this work provides a new insight into the electrochemical properties of PBAs and opens new perspectives to develop anode materials for rechargeable batteries.

1 Introduction

There is an urgent need for the development of efficient, safe and affordable energy storage devices for various technological applications, including mobile electronics, electric vehicles, and grid-scale energy storage systems[1-3]. Among the potential energy storage technologies, rechargeable lithium-ion batteries (LIBs) have attracted more and more attention around the world in recent years in view of their high energy density, simple maintenance, long cycle life and low weight[4-8]. However, the present lithium-ion battery technology is still not adequate. Accordingly, new battery chemistry needs to be developed to ensure large-scale and long-term applications, and to decrease battery management cost[9, 10].

Metal-organic frameworks, a new class of porous crystalline hybrid materials, formed by the linking of inorganic vertices (metal ions or clusters) and electron-donating organic ligands, have become a rapidly developing research area and attracted a tremendous amount of interest in the last two decades[11-13]. Owing to their high specific surface areas, controllable structures, adjusted pore sizes, combined with a low framework density and high thermal stability, MOFs act as outstanding candidates for potential uses related to clean energy, such as hydrogen energy, fuel cells, Li-ion rechargeable batteries, supercapacitors, solar cells and so on[14-19]. The redox of metal ions inside MOFs could provide a pathway for electrons. Alternatively, the open framework crystal structure allows highly reversible intercalation and extraction of ions with either aqueous or organic electrolytes. After the first report by Tarascon[20], the investigation of MOFs as electrode materials for rechargeable batteries has been expanding and raised broad interests. In particular, Prussian blue and its analogues have been intensively studied as the possible candidates[21, 22]. Cui' group[23] has recently reported reversible insertion/extraction of sodium and potassium ions in Prussian blue analogue nickel hexacyanoferrate electrode materials for at least 5000 cycles at high current densities in low-cost aqueous electrolytes, also the copper-nickel alloy hexacyanoferrate nanoparticles[24]. Especially, the copper hexacyanoferrate exhibited excellent capacity retention with extremely high rate capability, even at an ultra-high discharge rate of 83C, 67% of its maximum discharge capacity was observed[25]. Goodenough and co-workers[26] synthesized $KMFe(CN)_6$ compounds (M = Mn, Fe, Co, Ni and Zn) at room temperature and investigated the electrochemical behavior as cathodes for a rechargeable sodium-ion battery. Besides, they recently synthesized rhombohedral $Na_{1.72}MnFe(CN)_6$ through a facile solution precipitation route[27]. The resultant materials exhibited high reversible capacity of 134 mAh g^{-1} at a current density of 0.05C with outstanding rate capability. A thin film electrode of $Na_{1.32}Mn[Fe(CN)_6]_{0.83} \cdot 3.5H_2O$ exhibited two plateaus at 3.3 V and 3.6 V *vs.* Na$^+$/Na in the charge curve, resulting a high capacity of 109 mAh g^{-1} at 0.5C and good cyclability[28]. Very recently, binary and ternary Prussian blue analogue composites have been studied to overcome the disadvantages of limited capacity and cycle stability as cathode materials for Li-ion batteries[29-31]. However, there are still some aspects should be noticed. Most works based on Prussian blue or its analogues reported the cathode properties of the host framework for rechargeable batteries, which prompted us to think that Prussian

blue analogues may also perform well in electrochemical performance as anode materials.

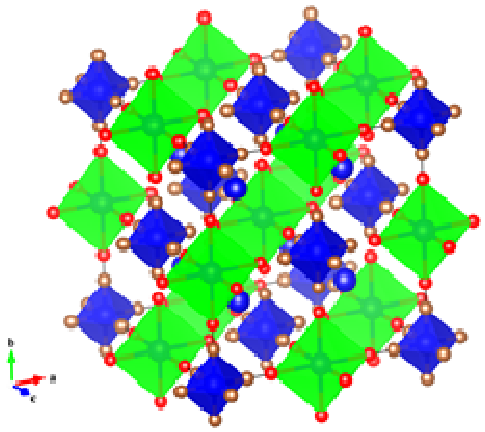

Fig. 1 Schematic illustration of the crystal structure of Prussian blue analogue $Co_3[Co(CN)_6]_2$.

In this work, we report the facile synthesis $M_3^{II}[Co^{III}(CN)_6]_2 \cdot nH_2O$(M=Co, Mn) nanocubes using a solution precipitation method, and the investigation of the host framework as anode materials for Li-ion batteries has been carried out for the first time. Benefiting from the open framework structure and nanoparticle morphology, the $Co_3[Co(CN)_6]_2$ exhibits a very high capacity of 566.2 mAh g^{-1} and excellent rate capacity (102.7 mAh g^{-1}, even at a very high current density of 2 A g^{-1}).

2 Experimental

Materials Synthesis

All chemicals are of analytical grade and used without further purification. The preparation of $M_3[Co(CN)_6]_2$ (M=Co, Mn) nanoparticles is based on a reported method with some modifications[32, 33]. In the typical synthesis procedure of $Co_3[Co(CN)_6]_2$, 0.08 mmol $K_3[Co(CN)_6]_2$ and 0.6 g SDBS were dissolved in 20 mL deionized water under vigorous stirring to form a clear solution. Meanwhile, 0.15 mmol $Co(CH_3COO)_2 \cdot 4H_2O$ was added into 20 mL pure water to prepare another clear solution. Then, the $Co(CH_3COO)_2 \cdot 4H_2O$ solution was added into the above solution drop by drop slowly using a syringe. After that, the reaction was aged at room temperature for 24 h. At the end of the reaction, the resulting pink precipitation was collected by centrifugation and washed several times with distilled water and finally dried in a vacuum oven at 30 ℃. For the synthesis of $Mn_3[Co(CN)_6]_2$ Prussian blue analogues nanoparticles, the procedure was similar to that of the preparation of $Co_3[Co(CN)_6]_2$. Typically, 0.075 mmol $Mn(CH_3COO)_2 \cdot 4H_2O$ and 0.3 g polyvineypirrolydone (PVP, K30) were dissolved in 20 mL water/ethanol mixed solvent(1:3, v/v). Separately, 0.04 mmol $K_3[Co(CN)_6]_2$ was added into 10 mL deionized water to form a homogeneous solution. After stirring for 20 min, the two solutions were mixed together and aged at room temperature for 24 h. The white product was then collected by centrifugation and rinsed several times with distilled water and finally dried under vacuum at 30 ℃.

Materials Characterization

The morphologies and structures of the products were characterized with field-emission scanning electron microscopy (FESEM, LEO 1430VP, Germany) and transmission electron microscopy (HRTEM, JEOL JEM-2010). The composition of the samples was analyzed by energy dispersive X-ray spectroscopy (EDS) attached to the SEM instrument. The powder X-ray diffraction (XRD) pattern was collected on a Bruker D8 Advance diffractometer equipped with Cu Kα radiation over the 2θ range of 10-80°. FTIR analysis of the sample was recorded on a Nicolet 750 Fourier transform infrared spectrometer using the KBr pellet method. Thermogravimetric analysis was carried out under air flow from 30 to 700 ℃ with a temperature ramp of 10 ℃ min^{-1}.

Electrochemical Measurements

The working electrode was prepared by casting a slurry of 80 wt% $M_3[Co(CN)_6]_2$ (M=Co, Mn) nanoparticles, 10 wt% acetylene black, and 10 wt% poly(vinylidene difluoride) in N-methyl-2-pyrrolidinone on a copper foil. Cells were assembled using standard 2016 coin-type cells in an argon filled glove-box, with lithium foil as both the counter and reference electrode, the polypropylene membrane (Celgard 2400) served as separator. The electrolyte used was 1.0 M $LiPF_6$ in a 1:1 mixture by volume of ethylene carbonate and dimethyl carbonate (EC/DMC). Galvanostatic charge/discharge cycles were performed on a LAND 2001A Battery Tester between 0.01-3.00 V at various current densities. Cyclic voltammetry measurements were carried out on an electrochemical workstation (CHI750D) in the potential range of 0.01-3.00 V *vs.* Li^+/Li at a scan rate of 0.1 mV s^{-1}.

3 Results and discussion

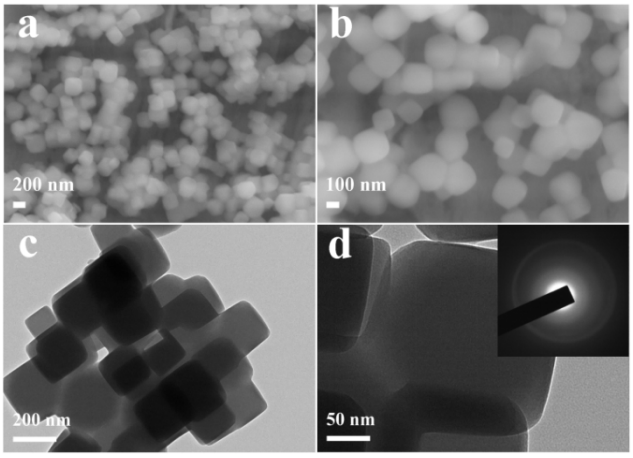

Fig. 2 Typical FESEM (a, b) and TEM (c, d) images of as-prepared $Co_3[Co(CN)_6]_2 \cdot nH_2O$ nanocubes. Inset in (d): the corresponding SAED pattern.

$Co_3[Co(CN)_6]_2$ is a typical Prussian blue analogue with the chemical formula $M_3^{II}[M^{III}(CN)_6]_2 \cdot yH_2O$ (M represents transition metals). In the crystal structure, octahedral $Co^{III}(CN)_6^{3-}$ complexes are bridged into a simple cubic lattice by Co^{2+} ions, forming a face-centred cubic phase (Fig. 1). The blue and dark yellow balls stand for Co and C atoms and the red balls represent N atoms, respectively[34, 35]. This framework could offer channels for ion and small molecule insertion, allowing rapid transport of these ions throughout the lattice. Importantly, zeolitic water in the interstitial sites within the

framework and on vacant nitrogen sites can also facilitate ion insertion.[19]

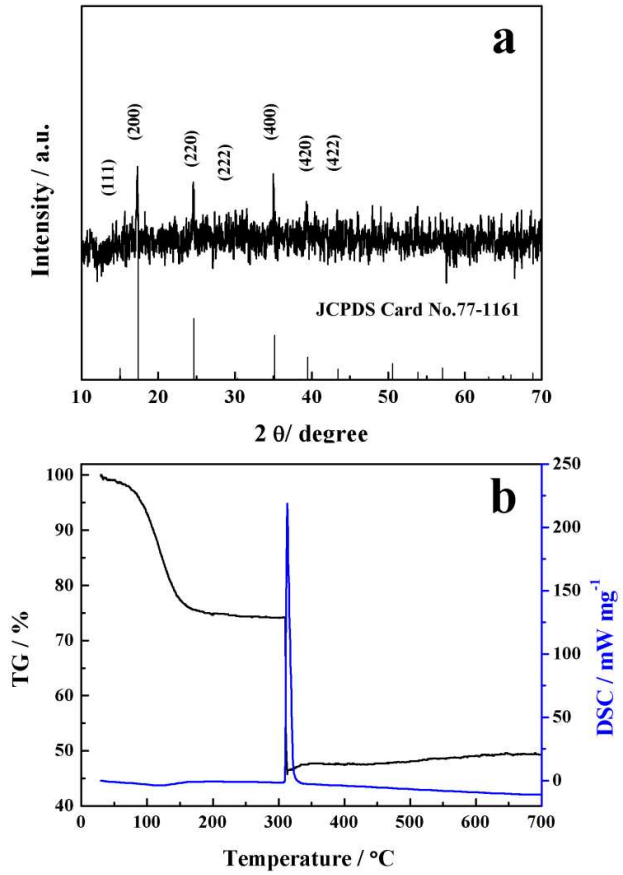

Fig. 3 XRD pattern of $Co_3[Co(CN)_6]_2{\cdot}nH_2O$ and thermogravimetric curve of the $Co_3[Co(CN)_6]_2$ sample at a rate of 10 ℃ min^{-1} in air.

The morphology and structure of the resultant $Co_3[Co(CN)_6]_2$ were observed by field emission scanning electron microscopy (FESEM) and transmission electron microscopy (TEM). As shown in Fig. 2a and b, the $Co_3[Co(CN)_6]_2$ are all well-defined nanocubes with a uniform edge length of around 200-300 nm. The size distribution of the $Co_3[Co(CN)_6]_2$ nanoparticles was shown in Fig. S1. For the samples more than 210 randomly selected particles were measured, taken from SEM images of different areas, using *Nano Measurer 1.2* software[36]. The average size and standard deviation are 222.54±39.98 nm for the $Co_3[Co(CN)_6]_2$ nanocubes. Further insight into the microstructures of the nanocubes is revealed from TEM analysis. Fig. 2c clearly shows the cube-like structures of $Co_3[Co(CN)_6]_2$, which is in good agreement with the FESEM observation. The high resolution TEM in Fig. 2d reveals the solid and dense texture of the $Co_3[Co(CN)_6]_2$ nanocubes. The selected-area electron diffraction pattern (the inset in Fig. 2d) from a single grain indicates the sample is polycrystalline in nature. In addition, EDS mapping further confirms that three elements Co, C, and N are distributed homogeneously throughout the samples; no other impurity elements were observed in the nanocubes (Fig. S2).

The crystal structure of the as-synthesized Prussian blue analogue was analyzed by X-ray diffraction (XRD), shown in Fig. 3a. All reflections can be well indexed into cubic $Co_3[Co(CN)_6]_2{\cdot}nH_2O$ with a space group of $Fm3m$[37, 38]. The lattice constant obtained is a = 10.2 Å, which agrees well with existing literature of $Co_3[Co(CN)_6]_2$ and JCPDS card no. 77-1161[39]. There is no evidence in the XRD pattern for the presence of other phase or impurities. FTIR spectrum also confirms the composition of $Co_3[Co(CN)_6]_2{\cdot}nH_2O$ sample. The absorption peak at 2174 cm^{-1} corresponds to the stretching vibrations from CN^- and the peak at 1611 cm^{-1} can be assigned to the stretching mode of OH, respectively (Fig. S3)[40]. From the thermogravimetric analysis (TGA) curve shown in Fig. 3b, the water content in the $Co_3[Co(CN)_6]_2{\cdot}nH_2O$ sample is calculated to be approximately 26 wt%, which corresponds to 11 water molecules per host lattice. The chemical composition of the sample can thus be expressed as $Co_3[Co(CN)_6]_2{\cdot}11H_2O$.

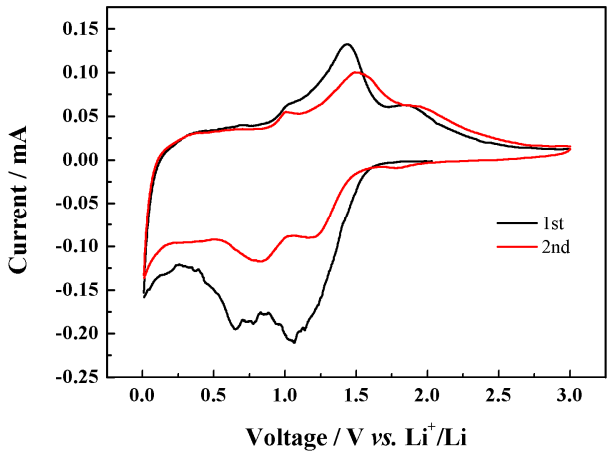

Fig. 4 CV curves of $Co_3[Co(CN)_6]_2{\cdot}nH_2O$ electrode at a scan rate of 0.1 mV s^{-1} between 0.01 and 3.0 V.

Motivated by the unique structural features, $Co_3[Co(CN)_6]_2{\cdot}11H_2O$ nanocubes were used to fabricate a new anode material for Li-ion batteries. Fig. 4 presents cyclic voltammograms (CV) in the first two cycles of the $Co_3[Co(CN)_6]_2$ electrode at a scan rate of 0.1 mV s^{-1} over the potential window of 0.01-3.00 V *vs.* Li/Li^+. In the first scan, two peaks were observed at *ca.* 0.65 and 1.06 V for $Co_3[Co(CN)_6]_2$, corresponding to the electrochemical reduction (lithiation) reaction of $Co_3[Co(CN)_6]_2$ with Li and possibly due to the formation of a solid electrolyte interphase (SEI). During the subsequent cycles, the main features in the CV curves appeared as three pairs of well-defined symmetric redox bands at 0.83/1.02 V, 1.23/1.44 V and 1.78/1.88 V, respectively, similar to the CV responses of Prussian blue and its analogues in earlier reports[41-44]. In one recent study, Cui *et al.*[45] reported the use of manganese hexacyanomanganate (Mn^{II}-N≡C-$Mn^{III/II}$) open-framework as an anode material for aqueous electrolyte battery. The authors concluded that the redox behaviour of manganese hexacyanomanganate proceeds by the following mechanisms:

$Mn^{III}[Mn^{III}(CN)_6] + A^+ + e^- = AMn^{II}[Mn^{III}(CN)_6]$ E^0=0.7 V vs. SHE (1)

$AMn^{II}[Mn^{III}(CN)_6] + A^+ + e^- = A_2Mn^{II}[Mn^{II}(CN)_6]$ E^0=0.0 V vs. SHE (2)

$A_2Mn^{II}[Mn^{II}(CN)_6] + A^+ + e^- = A_3Mn^{II}[Mn^{I}(CN)_6]$ E^0=-0.7 V vs. SHE (3)

Based on previous investigation on Prussian blue analogues and the different coordination sites of the Co ions, we therefore speculate that the peaks at 1.78/1.88 V correspond to oxidation/reduction of the Co^{III}/Co^{II} couple bonding to the N atoms of $C{\equiv}N^-$ and those at 1.23/1.44 V, 0.83/1.02 V to the

Co^{III}/Co^{II} and Co^{II}/Co^{I} couples coordinated with $C\equiv N^-$ by C atoms, respectively[26, 40, 44]. In the second cycle, the reduction peak is shifted to a higher potential at about 0.8 and 1.2 V while the oxidation peak position exhibits little change in the first two cycles. At present, the mechanism has not been fully elucidated; ongoing experiments with Fourier Transform Infrared Spectroscopy, X-ray photoelectron spectroscopy, and X-ray diffraction will provide a more complete understanding of the insertion reaction in this open framework.

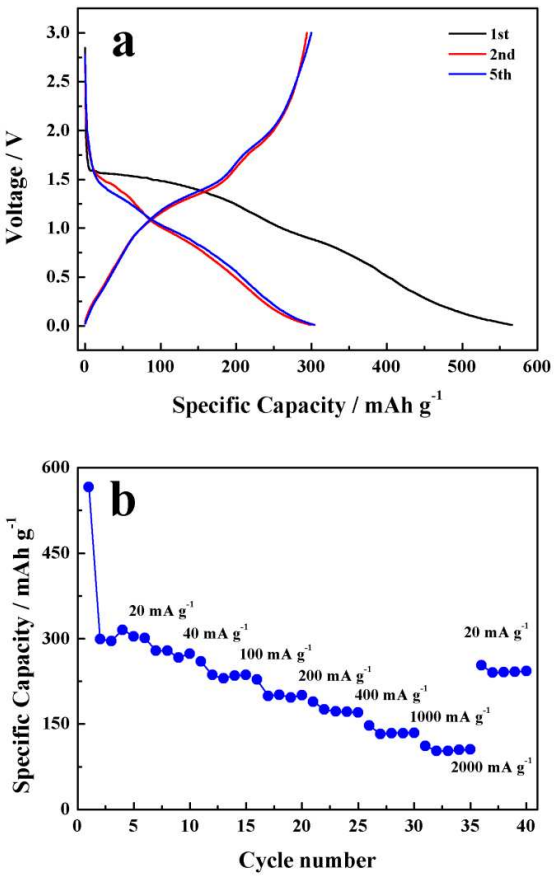

Fig. 5 (a) Discharge/charge curves of the $Co_3[Co(CN)_6]_2{\cdot}nH_2O$ in the voltage range of 0.01-3 V *vs.* Li/Li^+ at a current density of 20 mA g^{-1}, (b) Cycling performance of $Co_3[Co(CN)_6]_2{\cdot}nH_2O$ electrode at various current densities.

Figure 5a shows discharge/charge profiles of $Co_3[Co(CN)_6]_2{\cdot}11H_2O$ electrode for the first five cycles, in which the operating cutoff voltages are 0.01 and 3.0 V at a constant current density of 20 mA g^{-1}. Notably, the initial discharge exhibits a well-defined voltage plateau at about 1.5 V, followed by a long sloping curve down to the voltage of 0.01 V, which shifts to about 1.0 V and tends to be stable in subsequent cycles. Meanwhile, a poorly defined plateau is observed in the charge process at *ca.* 1.0-1.5 V. The first discharge and charge capacities of the $Co_3[Co(CN)_6]_2{\cdot}nH_2O$ are observed to be 566.2 and 294.2 mAh g^{-1}, respectively. The low Coulombic efficiency of 52% during the first cycle may result from irreversible capacity loss, including inevitable formation of solid electrolyte interface (SEI) and decomposition of electrolyte, which is common to most anode materials[13, 46]. Since the second cycle, the charge/discharge profiles are basically invariable. After five discharge/charge cycles, it exhibits a high reversible capacity of 304 mAh g^{-1}, and the columbic efficiency is remarkably increased to 101.3%, indicating high charge/discharge reversibility and good cycling stability of the $Co_3[Co(CN)_6]_2{\cdot}nH_2O$ nanocubes[47].

The high rate capability of material is an important parameter for LIBs in the practical application for fast discharging/charging. Fig. 5b shows the rate performance of the $Co_3[Co(CN)_6]_2$ electrode at various current densities over the potential range of 0.01-3.0 V. The electrode delivers reversible capacities of 299.1, 278.5, 235.9, 199.0, 175.6, and 132.5 mAh g^{-1} at current densities of 0.02, 0.04, 0.1, 0.2, 0.4, and 1 A g^{-1}, respectively, and finally recovered to around 253.0 mAh g^{-1} at 0.02 A g^{-1}. Even at a high current density of 2.0 A g^{-1}, a capacity more than 100 mAh g^{-1} could be delivered, corresponding to 34% of its maximum low rate capacity (0.02 A g^{-1}). This outstanding performance of the $Co_3[Co(CN)_6]_2$ electrode could be attributed to the synergistic effect of the open framework structure combined with small particle sizes of the material, which facilitate the electrolyte penetration and Li ions transportation in the electrode.

Eftekhari[48] reported a solid-state secondary battery based on chromium hexacyanochromate anode and chromium hexacyanoferrate cathode, respectively. The cell delivered a specific capacity of *ca.*8 mAh at a current density of C/11, and similar performance for iron hexacyanochromate anode.[49] Importantly, the author then successfully fabricated a high-voltage thin-film secondary cell based on chromium hexacyanochromate anode and Prussian blue cathode.[50] When eight unit cells were connected in series, the operating voltage of ~20 V can be increased to reach the values required for various technological applications. The results reported are of interest for the preparation of microbatteries with specified properties. However, those batteries had poor mass-balancing which resulted in overcharge of one electrode and rapid capacity loss. Very recently, Pasta *et al.*[45] reported a new symmetric open-framework cell in an aqueous electrolyte (10 M $NaClO_4$). This type of aqueous electrolyte battery relies on the insertion of sodium ions into the copper hexacyanoferrate cathode and a newly developed manganese hexacyanomanganate anode. The battery delivers a reversible capacity of about 28 mAh g^{-1} at a 1C rate, and exhibits remarkable capacity retention at high current rates. Equally impressive is the long term cycle life. There was no measurable capacity loss after 1000 cycles at a 10 C rate. In addition, the electrochemical behaviour of $Co_3[Co(CN)_6]_2$ is comparable with the results of other metal-organic framework anodes from the literature.[51-55]

Compared to inorganic anode materials, $Co_3[Co(CN)_6]_2$ offers some unique advantages: (1)$Co_3[Co(CN)_6]_2$ can be obtained using inexpensive and high-yield synthesis methods at room temperature, easy scalability for industrial application. Owing to facile control of the morphology and size of Prussian blue analogues by varying process parameters, various kinds of $Co_3[Co(CN)_6]_2$ with diverse architectures and morphologies can be synthesized.[38] (2)Currently, functional materials comprising binary, ternary and more complex structures and configurations are gaining increasing attention due to their unique physical and chemical properties in rechargeable batteries and supercapacitors.[31, 56] For most PBAs, the crystal structures and lattice constants are close to each other. Therefore, it is possible to synthesize Prussian blue analogue $Co_3[Co(CN)_6]_2$ with heterogeneous structures by epitaxial growth.[37, 57] (3)The open-framework structure of Prussian blue analogues allows rapid

insertion and removal of Na^+, K^+, Mg^{2+} and other ions with little lattice strain because of its large channels and interstices, [19, 45]which may make $Co_3[Co(CN)_6]_2$ promising candidates for future application in polyvalent ion batteries, including magnesium and aluminum ion batteries.

Success with Li ion insertion has motivated us to explore other Prussian blue analogue materials for Li insertion. $Mn_3[Co(CN)_6]_2{\cdot}nH_2O$ was also synthesized following the procedure reported[33], and its shape was observed by SEM. As shown in Fig. S4a, uniform $Mn_3[Co(CN)_6]_2$ with the size around 300 nm were obtained at room temperature. Cyclic voltammograms show reversible insertion of Li^+ ions in a non-aqueous electrolyte (Fig. S4b). The $Mn_3[Co(CN)_6]_2$ could deliver high initial capacity of over 868.2 mA h g^{-1} in the voltage window of 0.01-3 V at a current density of 50 mA g^{-1}. From the second cycle, $Mn_3[Co(CN)_6]_2$ nanocubes exhibit high capacities of 354.9 mAh g^{-1} (Fig. S4c). However, the materials suffer from an abrupt capacity fading with increasing cycle number, with a value of 35.3 mAh g^{-1} after 100 cycles, which is a common problem for Prussian blue analogues (Fig. S4d)[29, 31, 40].

Conclusions

In the present work, we have demonstrated, for the first time, the synthesis of Prussian blue analogue $M_3[Co(CN)_6]_2$ (M=Co, Mn) and its electrochemical performance as a new anode material for rechargeable Li-ion batteries. The as-prepared $Co_3[Co(CN)_6]_2{\cdot}nH_2O$ material can deliver a reversible capacity of 299.1 mAh g^{-1} with high Coulombic efficiency, and good capacity retention with increased current densities. Even at 2 A g^{-1}, a capacity of 102.7 mAh g^{-1} can be obtained, demonstrating superior rate capability and excellent cycling stability. The open-framework structure of $Co_3[Co(CN)_6]_2{\cdot}nH_2O$ allowed rapid transport of Li^+ ions through large channels, which resulted in an excellent rate capability. Considering their simple, facial synthesis and great performance, we believe that the novel Prussian blue analogues with fascinating lithium storage properties can be promising anode candidates for future application in Li-ion batteries. Our results may open up the way for the usage of MOFs toward future development in sodium ion (Fig. S5) and divalent ion batteries.

Acknowledgements

This work is financially supported by the National Program on Key Basic Research Project of China (973 Program, No. 2014CB239701), National Natural Science Foundation of China (No. 21173120, 51372116) and Natural Science Foundations of Jiangsu Province (No.BK2011030).

Notes and references

College of Material Science and Engineering, Nanjing University of Aeronautics and Astronautics, Nanjing, China, Fax: +86 025 52112626; Tel: +86 025 52112918; E-mail: azhangxg@163.com

Electronic Supplementary Information (ESI) available: [supplementary figures: size distribution histograms, elemental mapping images, FTIR spectrum, SEM image and electrochemical performance]. See DOI: 10.1039/b000000x/

1. Y. Li, M. Gong, Y. Liang, J. Feng, J.-E. Kim, H. Wang, G. Hong, B. Zhang and H. Dai, *Nat. Commun*, 2013, **4**, 1805.
2. Z. Wei Seh, W. Li, J. J. Cha, G. Zheng, Y. Yang, M. T. McDowell, P.-C. Hsu and Y. Cui, *Nat. Commun*, 2013, **4**, 1331.
3. Q. Zhang, E. Uchaker, S. L. Candelaria and G. Cao, *Chem. Soc. Rev.*, 2013, **42**, 3127-3171.
4. P. Nie, L. Shen, F. Zhang, L. Chen, H. Deng and X. Zhang, *CrystEngComm*, 2012, **14**, 4284-4288.
5. L. Shen, E. Uchaker, X. Zhang and G. Cao, *Adv. Mater.*, 2012, **24**, 6502-6506.
6. L. Shen, H. Li, E. Uchaker, X. Zhang and G. Cao, *Nano Lett.*, 2012, **12**, 5673-5678.
7. L. Wang, Z. Schnepp and M. M. Titirici, *J. Mater. Chem. A*, 2013, **1**, 5269-5273.
8. J. Popovic, R. Demir-Cakan, J. Tornow, M. Morcrette, D. S. Su, R. Schlögl, M. Antonietti and M.-M. Titirici, *Small*, 2011, **7**, 1127-1135.
9. S.-T. Myung, M. Kikuchi, C. S. Yoon, H. Yashiro, S.-J. Kim, Y.-K. Sun and B. Scrosati, *Energy Environ. Sci.*, 2013, **6**, 2609-2614.
10. H. Pan, Y.-S. Hu and L. Chen, *Energy Environ. Sci.*, 2013, **6**, 2338-2360.
11. Y. Yue, Z.-A. Qiao, P. F. Fulvio, A. J. Binder, C. Tian, J. Chen, K. M. Nelson, X. Zhu and S. Dai, *J. Am. Chem. Soc.*, 2013, **135**, 9572-9575.
12. W. Xia, B. Qiu, D. Xia and R. Zou, *Sci. Rep.*, 2013, **3**.
13. L. Zhang, H. B. Wu and X. W. Lou, *J. Am. Chem. Soc.*, 2013, **135**, 10664-10672.
14. G. Xu, B. Ding, L. Shen, P. Nie, J. Han and X. Zhang, *J. Mater. Chem. A*, 2013, **1**, 4490-4496.
15. S.-L. Li and Q. Xu, *Energy Environ. Sci.*, 2013, **6**, 1656-1683.
16. A. Morozan and F. Jaouen, *Energy Environ. Sci.*, 2012, **5**, 9269-9290.
17. R. Demir-Cakan, M. Morcrette, F. Nouar, C. Davoisne, T. Devic, D. Gonbeau, R. Dominko, C. Serre, G. Férey and J.-M. Tarascon, *J. Am. Chem. Soc.*, 2011, **133**, 16154-16160.
18. Y. Mizuno, M. Okubo, E. Hosono, T. Kudo, H. Zhou and K. Oh-ishi, *J. Phys. Chem. C*, 2013, **117**, 10877-10882.
19. R. Y. Wang, C. D. Wessells, R. A. Huggins and Y. Cui, *Nano Lett.*, 2013, **13**, 5748-5752.
20. G. Férey, F. Millange, M. Morcrette, C. Serre, M.-L. Doublet, J.-M. Grenèche and J.-M. Tarascon, *Angew. Chem. Int. Ed.*, 2007, **46**, 3259-3263.
21. H. Lee, Y.-I. Kim, J.-K. Park and J. W. Choi, *Chem. Commun.*, 2012, **48**, 8416-8418.
22. D. Asakura, M. Okubo, Y. Mizuno, T. Kudo, H. Zhou, K. Ikedo, T. Mizokawa, A. Okazawa and N. Kojima, *J. Phys. Chem. C*, 2012, **116**, 8364-8369.
23. C. D. Wessells, S. V. Peddada, R. A. Huggins and Y. Cui, *Nano Lett.*, 2011, **11**, 5421-5425.
24. C. D. Wessells, M. T. McDowell, S. V. Peddada, M. Pasta, R. A. Huggins and Y. Cui, *ACS Nano*, 2012, **6**, 1688-1694.
25. C. D. Wessells, R. A. Huggins and Y. Cui, *Nat. Commun*, 2011, **2**, 550.
26. Y. Lu, L. Wang, J. Cheng and J. B. Goodenough, *Chem. Commun.*, 2012, **48**, 6544-6546.
27. L. Wang, Y. Lu, J. Liu, M. Xu, J. Cheng, D. Zhang and J. B. Goodenough, *Angew. Chem. Int. Ed.*, 2013, **52**, 1964-1967.

28. T. Matsuda, M. Takachi and Y. Moritomo, *Chem. Commun.*, 2013, **49**, 2750-2752.
29. D. Asakura, C. H. Li, Y. Mizuno, M. Okubo, H. Zhou and D. R. Talham, *J. Am. Chem. Soc.*, 2013, **135**, 2793-2799.
30. X.-J. Wang, F. Krumeich and R. Nesper, *Electrochem. Commun.*, 2013, **34**, 246-249.
31. M. Okubo and I. Honma, *Dalton Trans.*, 2013, **42**, 15881-15884.
32. N. Yan, F. Wang, H. Zhong, Y. Li, Y. Wang, L. Hu and Q. Chen, *Sci. Rep.*, 2013, **3**.
33. L. Hu, P. Zhang, Q.-w. Chen, N. Yan and J.-y. Mei, *Dalton Trans.*, 2011, **40**, 5557-5562.
34. M. Cao, X. Wu, X. He and C. Hu, *Chem. Commun.*, 2005, **0**, 2241-2243.
35. S. Natesakhawat, J. T. Culp, C. Matranga and B. Bockrath, *J. Phys. Chem. C*, 2006, **111**, 1055-1060.
36. Y. Du, Y. Zhang, K. Huang, S. Wang, L. Yuan and S. Feng, *Dalton Trans.*, 2013, **42**, 8041-8048.
37. P. Nie, L. Shen, H. Luo, H. Li, G. Xu and X. Zhang, *Nanoscale*, 2013, **5**, 11087-11093.
38. L. Hu, P. Zhang, Q.-w. Chen, J.-y. Mei and N. Yan, *RSC Adv.*, 2011, **1**, 1574-1578.
39. N. Yan, L. Hu, Y. Li, Y. Wang, H. Zhong, X. Hu, X. Kong and Q. Chen, *J. Phys. Chem. C*, 2012, **116**, 7227-7235.
40. X. Wu, W. Deng, J. Qian, Y. Cao, X. Ai and H. Yang, *J. Mater. Chem. A*, 2013, **1**, 10130-10134.
41. K. Itaya, T. Ataka, S. Toshima and T. Shinohara, *J. Phys. Chem.*, 1982, **86**, 2415-2418.
42. K. Itaya, I. Uchida and V. D. Neff, *Acc. Chem. Res.*, 1986, **19**, 162-168.
43. A. A. Karyakin, *Electroanalysis*, 2001, **13**, 813-819.
44. A. Widmann, H. Kahlert, I. Petrovic-Prelevic, H. Wulff, J. V. Yakhmi, N. Bagkar and F. Scholz, *Inorg. Chem.*, 2002, **41**, 5706-5715.
45. M. Pasta, C. D. Wessells, N. Liu, J. Nelson, M. T. McDowell, R. A. Huggins, M. F. Toney and Y. Cui, *Nat. Commun*, 2014, **5**, 3007.
46. L. Yu, L. Zhang, H. B. Wu, G. Zhang and X. W. Lou, *Energy Environ. Sci.*, 2013, **6**, 2664-2671.
47. G. Zhang, B. Y. Xia, C. Xiao, L. Yu, X. Wang, Y. Xie and X. W. Lou, *Angew. Chem. Int. Ed.*, 2013, **52**, 8754-8754.
48. A. Eftekhari, *J. Power Sources*, 2003, **117**, 249-254.
49. A. Eftekhari, *J. Mater. Sci. Lett.*, 2003, **22**, 1251-1253.
50. A. Eftekhari, *J. Power Sources*, 2004, **132**, 291-295.
51. L. Gou, H.-X. Zhang, X.-Y. Fan and D.-L. Li, *Inorg. Chim. Acta*, 2013, **394**, 10-14.
52. X. Li, F. Cheng, S. Zhang and J. Chen, *J. Power Sources*, 2006, **160**, 542-547.
53. H. Chen, M. Armand, M. Courty, M. Jiang, C. P. Grey, F. Dolhem, J.-M. Tarascon and P. Poizot, *J. Am. Chem. Soc.*, 2009, **131**, 8984-8988.
54. P. C. Cheng, F. S. Tseng, C. T. Yeh, T. G. Chang, C. C. Kao, C. H. Lin, W. R. Liu, J. S. Chen and V. Zima, *CrystEngComm*, 2012, **14**, 6812-6822.
55. W. Walker, S. Grugeon, H. Vezin, S. Laruelle, M. Armand, F. Wudl and J.-M. Tarascon, *J. Mater. Chem.*, 2011, **21**, 1615-1620.
56. M. Okubo, C. H. Li and D. R. Talham, *Chem. Commun.*, 2014, **50**, 1353-1355.
57. M. Hu, A. A. Belik, M. Imura and Y. Yamauchi, *J. Am. Chem. Soc.*, 2012, **135**, 384-391.

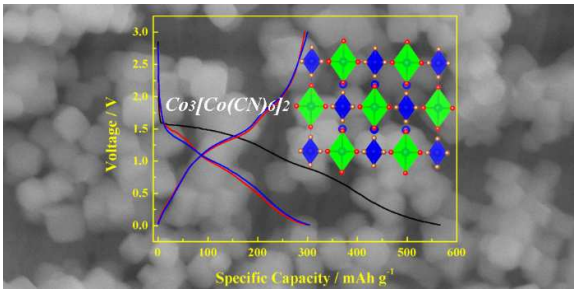

Herein, we demonstrate that nanoparticles of cobalt hexacyanocobaltate and manganese hexacyanocobaltate, typical Prussian blue analogues with the chemical formula $M_3^{II}[Co^{III}(CN)_6]_2 \cdot nH_2O$ (M=Co, Mn), can be operated as novel battery anodes in an organic liquid-carbonate electrolyte.